Device

Article

Luminal electrophysiological neuroprofiling system for gastrointestinal neuromuscular diseases

Graphical abstract

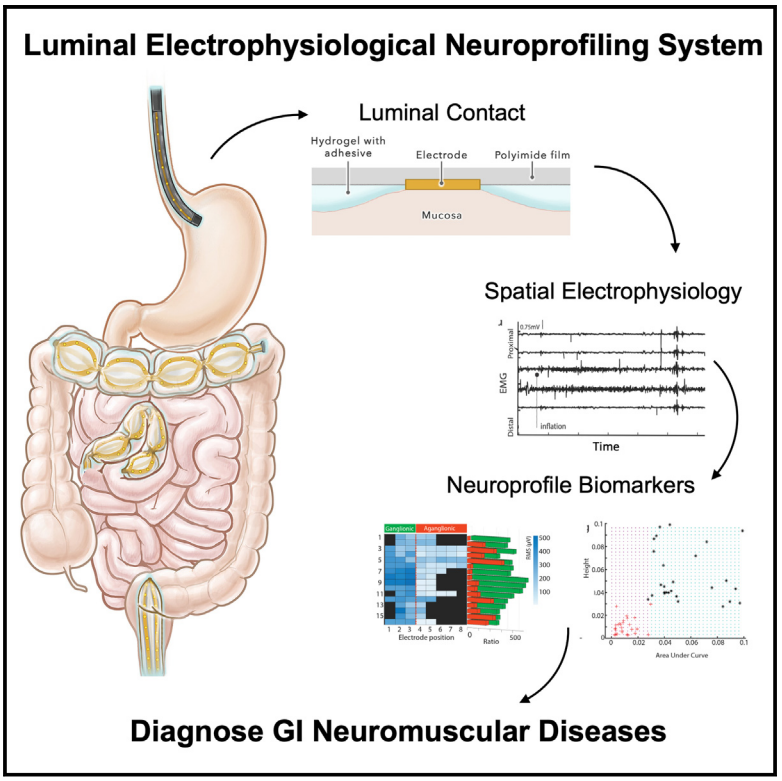

Highlights

- The LENS is a luminal electrophysiological neuroprofiling system
- The LENS electrophysiologically characterizes the GI tract for disease diagnosis
- Analytical metrics are generated to differentiate neuromuscular diseases
- High-resolution spatial profiles identify ganglionic-aganglionic transition zones

Authors

Shriya S. Srinivasan, Sabrina Liu, Ryo Hotta, ..., Niora Fabian, Allan M. Goldstein, Giovanni Traverso

Correspondence

shriyas_srinivasan@fas.harvard.edu (S.S.S.), amgoldstein@mgb.org (A.M.G.), cgt20@mit.edu (G.T.)

In brief

The luminal electrophysiological neuroprofiling system consists of an endoscopic device and series of biomarkers that characterize the electrical activity of the digestive tract to aid the diagnosis of gastrointestinal neuromuscular diseases. This study describes the device's development and validation and provides example cases of neuroprofiling to detect neuropathies and aganglionosis.

Develop
Prototype with demonstrated applications in relevant environment

Srinivasan et al., 2024, Device 2, 100400
July 19, 2024
https://doi.org/10.1016/j.device.2024.100400

CellPress

Device

CellPress
OPEN ACCESS

Article

Luminal electrophysiological neuroprofiling system for gastrointestinal neuromuscular diseases

Shriya S. Srinivasan,[1,2,3,6,*] Sabrina Liu,[3] Ryo Hotta,[4] Sukhada Bhave,[4] Amro Alshareef,[1,2,3] Binbin Ying,[1] George Selsing,[2,3] Johannes Kuosmanen,[1] Keiko Ishida,[3] Joshua Jenkins,[1] Wiam Abdalla Mohammed Madani,[3] Alison Hayward,[1,3,5] Niora Fabian,[1,5] Allan M. Goldstein,[4,*] and Giovanni Traverso[1,2,3,*]

[1]Department of Mechanical Engineering, Massachusetts Institute of Technology, Cambridge, MA 02139, USA
[2]Division of Gastroenterology, Hepatology and Endoscopy, Brigham and Women's Hospital, Harvard Medical School, Boston, MA 02115, USA
[3]David H. Koch Institute for Integrative Cancer Research, Massachusetts Institute of Technology, Cambridge, MA 02139, USA
[4]Department of Pediatric Surgery, Massachusetts General Hospital, Boston, MA 02114, USA
[5]Division of Comparative Medicine, Massachusetts Institute of Technology, Cambridge, MA 02139, USA
[6]Lead contact
*Correspondence: shriyas_srinivasan@fas.harvard.edu (S.S.S.), amgoldstein@mgb.org (A.M.G.), cgt20@mit.edu (G.T.)
https://doi.org/10.1016/j.device.2024.100400

THE BIGGER PICTURE Limited tools exist to electrophysiologically characterize the gastrointestinal (GI) system for the diagnosis of GI neuromuscular diseases, due to the challenging anatomical structure of the GI tract. The luminal electrophysiological neuroprofiling system consists of an endoscopic device and series of biomarkers that can create high-resolution spatial maps of the electrical activity in the digestive tract, aiding in the diagnosis of conditions such as GI dysmotility and weakness of the muscles involved in swallowing. The system may ultimately benefit clinicians, surgeons, and patients by improving diagnostic precision and tailoring treatment plans for individuals with GI disorders.

SUMMARY

Gastrointestinal (GI) neuromuscular diseases can be challenging to diagnose due to inadequate profiling technologies that are unable to pinpoint underlying pathology. We introduce a luminal electrophysiological neuroprofiling system (LENS). This tool uses high-resolution electromyographic data to capture motility of the GI tract, grade neurogenic deficiencies over time, and elucidate motility patterns. Through the development of analytical metrics, we determine "neuroprofiles" for various enteric neuropathies in models of dysmotility, sphincter dysfunction, and aganglionosis. The LENS differentiates between aganglionic and ganglionic regions based on the contractile rate ($p < 0.0001$) and root-mean-square amplitude ($p < 0.0001$). In mice with hypomotility, metrics like area under the curve and peak height of the Fourier transformation of the electrophysiological signal in the frequency ranges of 0–20 and 115–135 Hz were significant differentiators, with up to 89% accuracy of classification between pathologic and normal motility. Such a platform can enable realization of specific diagnoses and quantify their severity.

INTRODUCTION

Toward diagnostic specificity among GINMDs

Gastrointestinal (GI) neuromuscular diseases (GINMDs) encompass a heterogeneous set of debilitating motor and sensory disorders, posing a socioeconomic burden that exceeds fifty billion dollars annually.[1] Etiopathology involves dysfunction in one or a combination of the enteric neurons, glial cells, interstitial cells of Cajal, smooth muscle, or autonomic signaling mechanisms, either along the entire GI tract or in a specific region. Due to the frequent overlap of clinical symptoms (abdominal distention, bloating, nausea, vomiting, early satiety, and constipation) among different etiologies, specificity in pathophysiologic diagnosis can be challenging.[2] Thus, despite several well-defined GINMDs, such as esophageal achalasia, gastroparesis, and Hirschsprung disease,[3] over 50% of cases are categorized as "idiopathic" or "functional" diseases and treated generically to alleviate symptoms.[1,2,4] The ability to differentiate between neurogenic and myogenic pathologies, to classify based on severity, to define anatomic localization, and to generate a nosology of these conditions has significant diagnostic and integral therapeutic value.[2]

Limitations of current tools

Methods and tools used for diagnosing GINMDs are cumbersome, pose several functional limitations, and often yield

broad diagnoses that are treated through a pharmacologic trial-and-error process.[4] Histopathology can, in some cases, reveal morphologic alterations, although full thickness tissue samples are challenging to obtain for patients not undergoing surgery.[2] Manometry, indicative of contractile and pressurization patterns, is indiscriminate to underlying pathology and requires endoscopy.[5–7] Colonic manometry is performed in children and is purported to distinguish neuropathic and myopathic causes but requires colonoscopy to position the manometry catheter and is time-consuming. High-resolution manometry provides improved, highly spatially resolved maps of pressure with minimized motion artifact, although its clinical utility has not significantly increased[8] compared to lower-resolution methods. Its rigid sensors are uncomfortable, do not conform to the GI geometry, and are less durable than water-perfused sensors.[8] Gastric emptying studies are a useful indicator of emptying rate, although unreliable in predicting clinical response to intervention.[3,5,9] Small bowel motor function is particularly challenging to diagnose as current tools are unable to navigate through the curved and unpredictable path of the small intestine.[10–12] Abdominal ultrasonography and lactulose H_2 breath test are alternative methods,[3] although their clinical utility and normative data are yet to be defined.[3]

Potential utility and challenges of electrophysiology

The myoelectric signals of each GI organ serve as a fingerprint of the neuromuscular physiology—corresponding to motion, neuroreflexivity, and pacing.[13–17] While electrophysiology of the tract has been investigated since the 1920s, it is sparsely utilized as a clinical diagnostic.[3,18] Traditional gastrography using surface electrodes on the stomach has been correlated with arrhythmias and gastroparesis, although it is not the standard of care for diagnosis.[19] More recently developed high-resolution arrays are enabling body surface gastric mapping,[20] with normative values being established for the biomarkers of gastric function.[21] A few approaches have utilized 1–2 intraluminal electrodes that are advanced along the tract with concurrent surgical manipulation.[22,23] The development of high-resolution mapping and diagnostic criteria has been challenged by either the invasive nature of laparotomies required to localize electrodes or the low specificity and quality of data acquired from surface or luminal recording.[24–26] There exists an imminent need to develop clinically-appropriate electrophysiology tools and physiologically relevant metrics to functionally characterize and establish specific criteria for the diagnosis of GINMDs. In this study, we develop a luminal electrophysical neuroprofiling system (LENS) and validate its usability, navigation, and measurement capabilities in the esophagus and anorectal regions of swine. Utilizing murine models of Hirschsprung disease and neuronal nitric oxide synthase (nNOS) deficiency, we develop a set of analytic metrics relevant for neurointestinal disorders. We hypothesize that the LENS design will enable facile use and passage through the GI organs and stable contact with the lumen for recordings of electromyography. We predict that the metrics of contractility and root-mean-squared activity will enable differentiation between normal and diseased colonic neuromusculature.

RESULTS

A high-resolution LENS was developed with the functional requirements of (1) conforming to the highly curved anatomy of the GI tract (curvatures <0.05 cm^{-1}) with minimized perforation risk,[10,11] (2) maintaining strong luminal contact,[23,23] (3) enabling insertion and removal without abrasion of the mucosa, (4) withstanding deformation of the tract, and (5) recording electrophysiology with high signal-to-noise ratios (SNRs). The LENS manifests in three embodiments, suited for (1) straight segments of the tract, (2) curved segments of the tract, or (3) use as an endoscopic sheath. The straight embodiment features up to 32 contacts, spaced equally around the circumference and length of the device, and is folded in a configuration that prevents luminal contact on insertion. Once placed at the desired location, an inner balloon is inflated to unfold and hold the contacts firmly against the lumen (Figure 1A). Such a device cannot navigate the large curvatures of the coiling segments of the small and large intestine and impinges on tissue (Figure S1). Thus, a segmented structure was devised (Figure 1B). The length and number of segments was empirically assessed in porcine small intestine *ex vivo* and optimized to four 3.8-cm segments, each possessing a maximal distension of 2.3 cm, commensurate with the average luminal diameter of the small intestine of 2.2–2.5 cm.[27] This embodiment can bend around curvatures of up to K = 1.5 cm as demonstrated in porcine small intestine *ex vivo* (Figure S2). The third LENS embodiment consists of an endoscopic sleeve, enabling multimodal, image-guided clinical evaluation of any region accessible by endoscope featuring both EMG and pressure sensors (Figures 1C and 1D). The LENS can be inflated with air or saline until the system's impedance profile, at 1,000 Hz, measures values less than 1,000 ohms, indicating the strong luminal contact required for consistent electrophysiological signals (Figure 1J).

For the catheter embodiment, a tough hydrogel adhesive, composed of an interpenetrating network of polyacrylamide, alginate, and chitosan, is coated on the LENS. Activating upon contact with the mucosa, physical (topological entanglement) and chemical bonds (amide reaction)[28] with the mucosal tissues enable adherence to the mucosa, which helps reduce contact impedance, surpass motion artifacts,[25,26] and enhance the SNR of recorded signals (Figures 1D–1F and S1). The impedance at the electrode-mucosa interface is significantly reduced ($p < 0.01$, Student's two-tailed homoscedastic t test) when compared to a control uncoated LENS (Figures 1L and 1K). In *ex vivo* studies, the average impedance of electrodes with a control device was 1.74e−05 ± 1.4e−05 ohms, whereas coating improved the impedance to 5.81e−03 ± 5.5e−03 ohms. *In vivo*, the impedance was 1.24e−05 ± 3.1e−04 ohms without the adhesive gel and 7.79e−04 ± 5.1e−03 ohms with the gel. Further, due to increased adherence and shear forces at the tissue-mucosa interface, device motion was reduced by 10-fold. *Ex vivo*, 0.26 ± 0.21 N of force was required to move the uncoated device in the orthogonal direction to tissue, while 2.415 ± 1.294 N wass required for the coated device. *In vivo*, 0.22 ± 0.15 N of force was required to move the uncoated device, while 2.51 ± 0.86 N was required

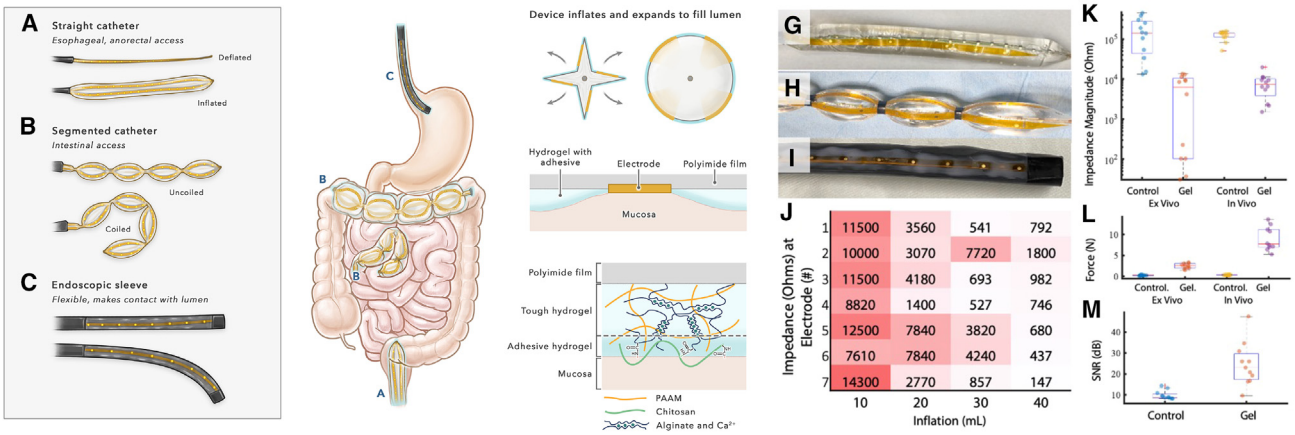

Figure 1. LENS embodiments and luminal contact

(A and G) Straight LENS for electrophysiological characterization of straight segments of the tract, such as the esophagus or regions of the distal colon, anus, and rectum.

(B and H) Segmented LENS configuration for profiling in the curved segments of the tract, including the intestines.

(C and I) Endoscopic sleeve embodiment of the LENS.

(D) Deflated geometry of the LENS for seamless insertion and optimal expansion for electrode-mucosa contact.

(E and F) Tough hydrogel coating enabling temporary attachment to the mucosa to improve mucosal contact and minimize motion.

(J) Heatmap of impedance; the segmented balloon was inflated to 40 mL in 10-mL increments, and the impedance of the seven electrodes (1,000-Hz screen) decreased following successful luminal contact.

(K) Magnitude of impedance in control and gel-coated devices. Impedance was scanned at 1,000 Hz.

(L) Adhesive force of the gel in *ex vivo* and *in vivo* swine esophagus with the control and gel-coated devices.

(M) Signal-to-noise ratio of EMG signals recorded on control and gel-coated LENS demonstrating significant improvements ($p < 0.001$, Student's t test) with enhanced mucosal adhesion. Scale bar in (G)–(I) represents 20 mm.

for the coated device (Figure 1L). These measurements characterize the adhesive aspect of the gel to the mucosa, suggesting that natural swallows and peristaltic motions of the tract will not cause a loss of contact or motion artifact on the device. Further, SNR of the electrophysiology was significantly ($p < 0.0001$, Student's two-tailed homoscedastic t test) improved with the gel-based adhesion from 9.81 ± 10.32 (control, $n = 8$ independent trials) to 24.61 ± 2.12 (gel, $n = 8$ independent trials, Figure 1M). Following use, after dissolution of the gel with 20 mL saline, the device can be detached from the mucosa with a gentle tug, 0.1–0.3 N of force.

Endoscopy was performed prior to and after usage of the LENS in the upper and lower esophagus and anorectal region. No mucosal abrasion or irritation or residual debris from the gel coating was observed due to LENS insertion, contact, and removal (Figures S3A and S3B). Histological analysis revealed no inflammation or mucosal injury (Figure S3C). All embodiments demonstrated integrity following cyclic inflation and deflation (up to 100 cycles), delamination testing, and repeated insertion processes in biological tissues ($n = 6$ swine) with less than 10% variance in the electrode's surface impedance. The endoscopic sleeve embodiment was tested in the esophagus of the swine and demonstrated efficacy in making luminal contact. Placement of electrodes against key structures, such as the lower esophageal sphincter, was able to be guided by the preceding endoscope. The flexibility and robustness of the sleeve was tested by flexing the endoscope tip through its full range of motion for 20 cycles. No contacts were damaged, and delamination did not occur (Figure S4).

Esophageal and anorectal electrophysiological characterization

Overcoming the challenges with luminal contact and insertion, we assessed the capability of the LENS to measure motility-related myoelectric activity. Following placement through the mouth into the upper esophagus, laryngeal stroking yielded reflexive swallows that were captured by sensors distal to the upper esophageal sphincter (UES) (Figure 2A). Simultaneous impedance planimetry corresponded with the measured peristaltic wave. SNR was always above 3.4. Then, a mechanical bolus was placed in the distal esophagus, generating brief regurgitation and spasm in the proximal esophagus. This was also captured by the electrophysiological device corresponding precisely with timing and luminal displacements (Figure 2B). We then placed the LENS at the lower esophageal sphincter. Inflation resulted in reflexive contraction at the sphincter. Injection of glucagon resulted in relaxation of the sphincter that was captured electrophysiologically by the suppression of muscle activity (Figure 2C). Following placement of the straight LENS in the rectal canal, a balloon was inserted proximally and inflated, inducing a rectal contraction. After a brief period in which the bolus descended in the tract, a defecatory contractile burst was observed, while the anus relaxed. These movements were captured by the LENS (Figure 2D). Although mucosal secretions pose a nominal barrier to the stabilization and clarity of signal acquisition by a luminally positioned device, SNRs did not diminish significantly during the 30-min recording window.

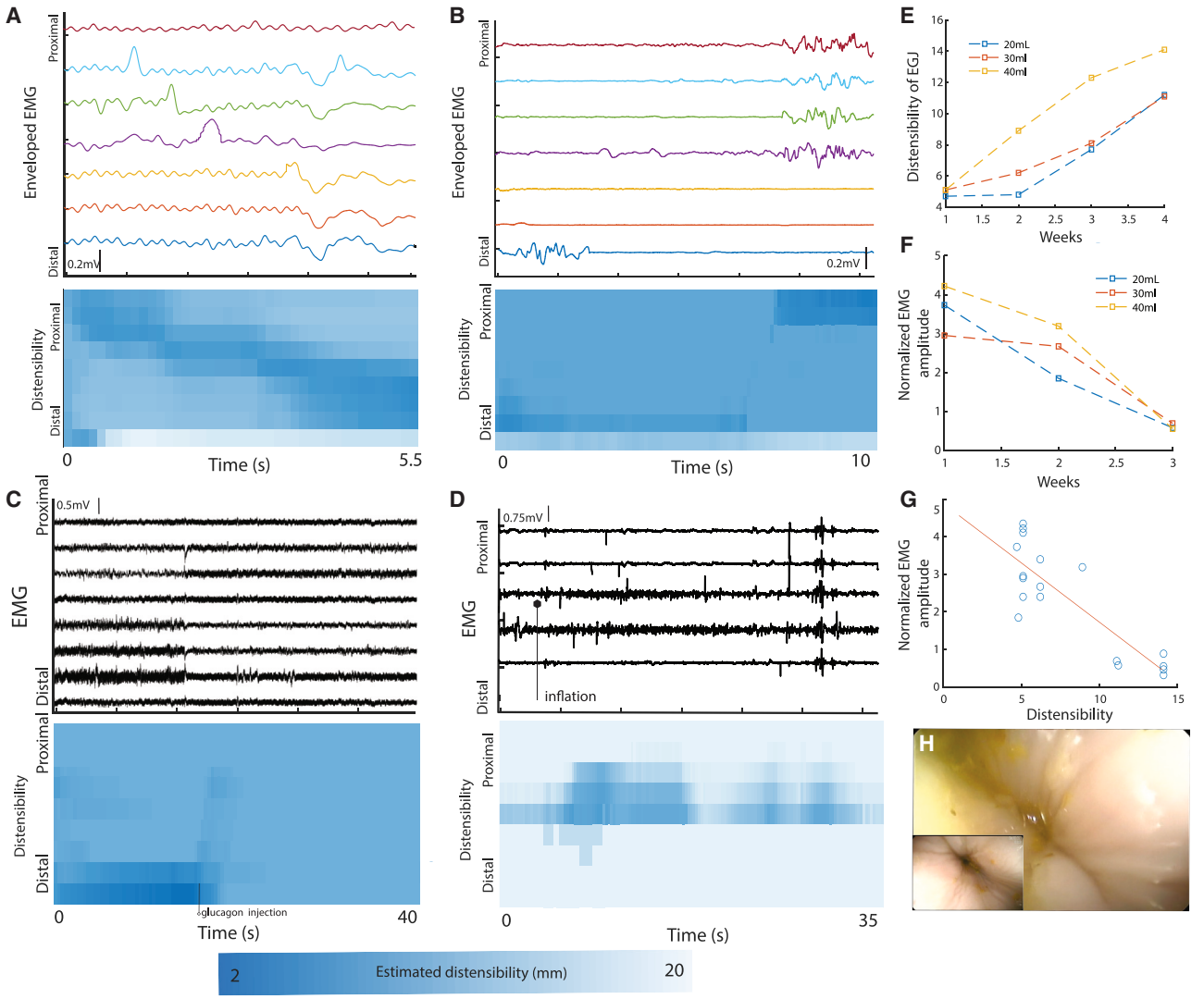

Figure 2. Esophageal and anorectal LENS characterization

(A and B) Enveloped EMG signals from a representative (A) esophageal swallow and (B) esophageal spasm.

(C and D) Raw EMG signals from (C) LES relaxation in response to glucagon and (D) an anorectal contraction in response to inflated balloon and attempts at evacuatory contraction.

(E) Distensibility of the esophageal-gastric junction in an animal model of GERD.

(F) Average EMG peak amplitudes during swallowing normalized to noise floor in an animal model of GERD.

(G) Comparison of distensibility and EMG amplitude demonstrates a linear relationship with correlation coefficient r = 0.72.

(H) Endoscopic view of the EGJ 4 weeks after botulinum toxin injection evinces loosening of the sphincter (inset) and reflux of gastric contents.

LENS profiling for sphincters

Beyond its use in recording patterns of peristalsis, contraction, and relaxation, we investigated the capability for the LENS to provide longitudinal evaluations of muscle contractility for use in diseases like gastrointestinal reflux disease (GERD). An animal model of GERD was created through injections of botulinum toxin into the four quadrants of the lower esophageal sphincter. Weekly luminal planimetry and electrophysiology demonstrated significant increases, over 3-fold the baseline, in distensibility of the esophageal-gastric junction (EGJ) consistent with prior reports[29] (Figure 2E). The development of GERD was also evinced by the presence of gastric contents that had been refluxed into the esophagus (Figure 2H). Using the LENS, the average peak EMG amplitudes elicited at the EGJ during natural or reflexively initiated swallows monotonically decreased 4-fold over the course of 4 weeks (Figure 2F). A comparison of the distensibility and strength of the EMG signal follows a linear trend (r^2 = 0.72), suggesting that the EMG amplitude can serve as a relevant marker for diagnosis or gradation of the neuromuscular dysfunction at the EGJ (Figure 2G).

We next investigated the ability of the LENS to measure baseline neuromuscular activity, indicative of components like

innervation, reflexivity, and baseline inhibition. We performed luminal recordings in two different murine models, developing metrics that (1) corresponded to physiological events or traits specific to the pathology of interest and (2) leveraged spectral analysis to perform classification of unlabeled data. This electrophysiological characterization was performed using a miniaturized version of the LENS device (20 mm long, 2 mm wide, consisting of 16 channels).

Localizing aganglionosis in Hirschsprung disease

Hirschsprung disease is a congenital disorder characterized by the absence of ganglion cells of the myenteric and submucosal plexuses of the terminal rectum and extending proximally for a variable distance.[30] Today, histological analysis is used to identify the transition zone (TZ) between aganglionic and normoganglionic bowel. However, the presence of ganglion cells does not necessarily correlate to normal motor function, and functional assessments are not available. As such, pull-through surgery is often complicated by remnant aganglionic or hypoganglionic segments that lead to persistent postoperative bowel dysfunction.[31] Anatomically precise localization of the TZ would ensure complete removal of this segment during surgery and pose significant therapeutic value.

Electrophysiology was performed using a miniaturized probe (described in the experimental procedures) in the distal 2.5–3 cm of the colon of endothelin receptor B (Ednrb)-deficient mice, an established model of Hirschsprung disease. Electrodes were positioned proximal and distal to the TZ to record the baseline activity for at least 20 min. The contractile rate, defined by the number of bursts per minute of recording, and the root-mean-square (RMS) amplitude were profiled with blinding to the location of the electrodes. After euthanasia, the position of each electrode was marked in the tissue. Staining for nestin and Tuj1, marking the enteric ganglia, revealed the TZ and allowed for classification of the electrodes as being in the aganglionic or ganglionic segment.

The contractile rate of the aganglionic segments (0.20 ± 0.11 bursts/minute) was significantly decreased compared to the ganglionic segment (0.46 ± 0.13 bursts/minute) ($p < 0.0001$, Student's two-tailed heteroscedastic t test) (Figures 3B and 3D). Similarly, the RMS amplitude of the aganglionic segments (105.11 ± 43.8 bursts/minute) was significantly decreased compared to the ganglionic segment (332.65 ± 97.20 bursts/minute) ($p < 0.0001$, Student's two-tailed heteroscedastic t test) (Figures 3C and 3E). The average contractile rate and RMS amplitude in each region were calculated on a per-trial basis and revealed an average aganglionic:ganglionic ratio of 0.37 ± 0.13 for the contractile rate and 0.28 ± 0.23 for the RMS amplitude (Figures 3D and 3E). Periodic stimulation was performed in separate trials ($n = 18$ trials, 10 min of recording after 1 min of stimulation each). Contractile rate was significantly increased in the ganglionic segments compared to the aganglionic segments (1.4–2.3 times the aganglionic rate, $p < 0.05$, Student's two-tailed heteroscedastic t test). A representative example is demonstrated in Figure 3F wherein electrodes 1 and 2 were in the ganglionic segment, while electrodes 3, 4, and 5 were in the aganglionic segment.

To assess the distinctiveness of the electrophysiological fingerprint of ganglionic and aganglionic segments, the frequency spectra were evaluated through classification-based strategies. The discrete Fourier transform (DFT) of the data was computed with a fast Fourier transform (FFT) algorithm and enveloped to reveal a bimodal distribution with peaks in the 0- to 20-Hz and 115- to 135-Hz regimes. Area under the curve (AUC) and peak height (PH) were determined for these ranges (Figure 3G). Principal component analysis revealed that 90% and 1.03% of the variability could be accounted for by the AUC and PH of the 0- to 20-Hz band, respectively (Figure 3H). K-means clustering was performed on these two components, unlabeled by their classification, (Figure 3I) generating two primary clusters centered at (1) x = 0.8731, y = 0.3010 and (2) x = 0.9305, y = 0.3175. To evaluate the accuracy of the autonomous clustering against the known classification, an adjusted Rand index was calculated. 89% of the recording locations could be accurately classified into the ganglionic or aganglionic segment using the AUC and PK metrics of the frequency spectra.

Together, the data and analytical methods demonstrate that the electrophysiological fingerprints of the ganglionic and aganglionic segments are significantly distinct, enabling reliable profiling of the level of ganglionosis in the colon. In this mouse model, this methodology enables determination of the TZ within 2 mm and could be replicated in the human colon within 0.5 cm by the LENS.

Fingerprinting enteric neuropathy

In addition to providing spatially relevant data, electrophysiological characterization can yield information regarding changes in electrical activity of GI smooth muscle in an animal model of enteric neuropathy. NO is an inhibitory neurotransmitter of non-adrenergic, noncholinergic enteric neurons that is synthesized from L-arginine by NOS. The null mutation of nNOS is associated with impaired relaxation of the lower esophageal and pyloric sphincters,[32] reduced relaxation in the ileum[33] and proximal colon,[34] and the absence of the rectoanal inhibitory reflex.[35] Mice lacking nNOS exhibit delayed gastric emptying as well as slow transit in the colon and have been used as a model of gastroparesis and mild constipation.[32,36,37]

Luminal electrophysiology of the distal 2.5–3 cm of the colon in wild-type (WT) and knockout (KO) nNOS mice (20 min, $n = 14$ animals/group) revealed significant differences in the contractile rate (WT = 0.82 ± 0.0177, KO = 0.482 ± 0.0155, $p < 0.001$, Student's two-tailed heteroscedastic t test) and RMS amplitude (WT = 61.909 ± 24.4, KO = 38.00 ± 9.33, $p < 0.0001$, Student's two-tailed heteroscedastic t test) (Figures 4A and 4B). Additionally, in response to periodic stimulation (10 Hz, 50 μA, 3 10-μs pulses for 90 s), the RMS amplitude of the WT group was significantly higher (WT = 154.38 ± 49.48, KO = 76.14 ± 28.74, $p < 0.001$, Student's two-tailed heteroscedastic t test) (Figure 4C).

Frequency spectra were analyzed to characterize profiles of neuronal reflexivity, revealing significantly greater magnitudes in the AUC and PH for each of the dominant frequency ranges for the KO group compared to the WT group ($p < 0.001$, Student's t test, Figures 4D, 4E, and 4F). These findings are commensurate with the underlying physiology of nNOS mice wherein the lack of nNOS leads to a hyperresponsive baseline condition with diminished relaxation and fewer coordinated

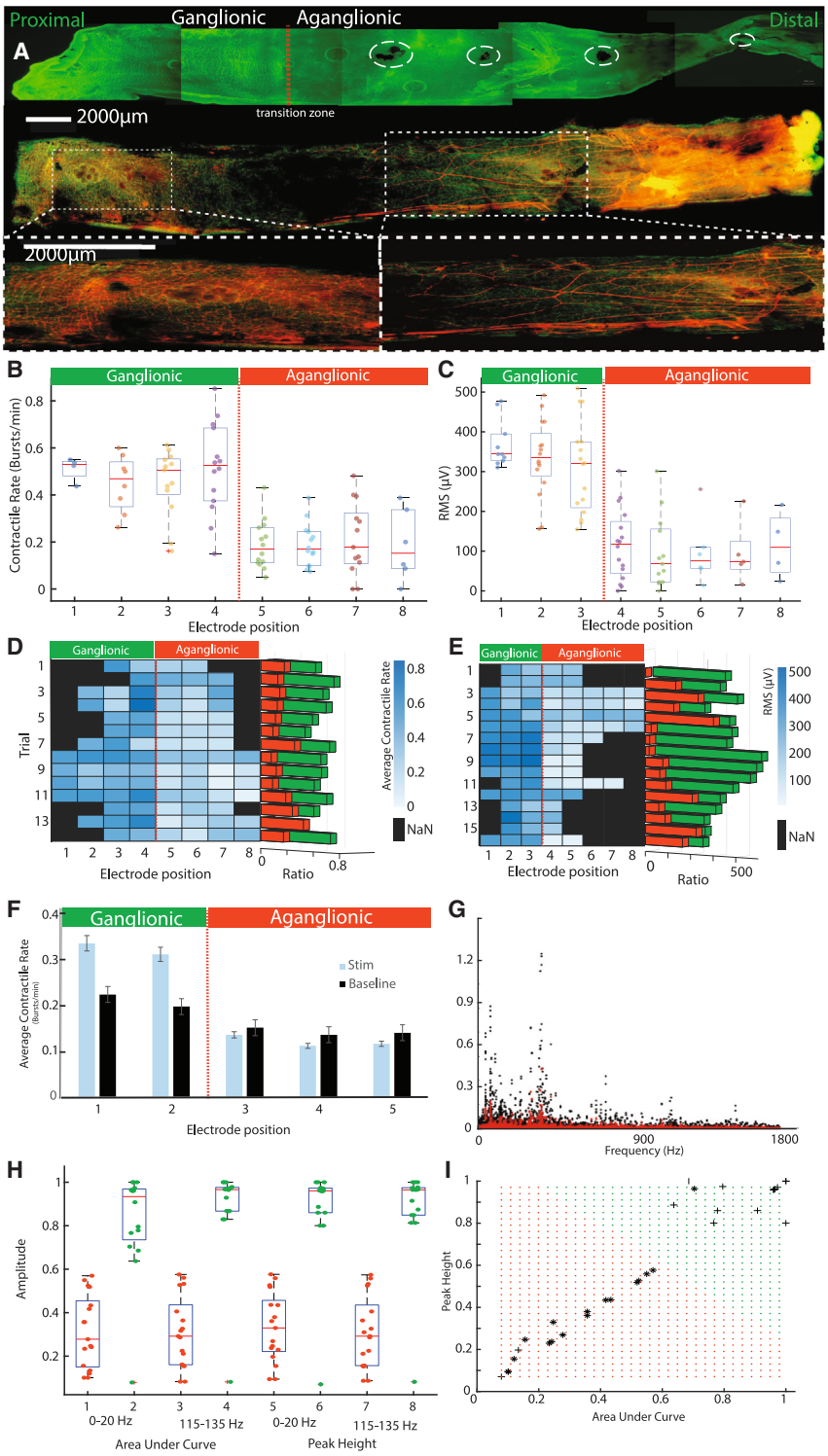

Figure 3. Electrophysiological profile of aganglionosis

(A) The rectoanal region of an Ednrb$^{-/-}$ mouse stained for Tuj1 and nestin-GFP identifies the transition zone by the sharp decrease in ganglia.

(B) The contractile rate (bursts/min) of electrodes positioned in the ganglionic region (1–4) was significantly higher than that in the aganglionic region (5–8) ($p < 0.0001$, Student's two-tailed heteroscedastic t test).

(C) The RMS amplitude of the EMG was significantly higher in each ganglionic electrode position (1–3) than each aganglionic electrode position (4–8) ($p < 0.0001$, Student's two-tailed heteroscedastic t test).

(D and E) Heatmap and bar chart of the ratio of contractile rate (D) and RMS (E) demonstrate the longitudinal point of differentiation and ratio of amplitudes for each animal.

(F) The average contractile rate was significantly greater during stimulation compared to baseline in the ganglionic region when compared to the aganglionic region ($p < 0.0001$, Student's two-tailed heteroscedastic t test).

(G) Fourier transformation of the signals demonstrates a heightened signal in the ganglionic regions (black) compared to the aganglionic segments (red).

(H) Area under curve and peak heights under the frequency ranges of 0–20 and 115–135 Hz for the WT and KO groups. Orange and green dots represent data from the aganglionic and ganglionic segments, respectively.

(I) K-means clusters demonstrate two separate regions with 89% accuracy of classification.

contractions. Principal components analysis of the AUC and PH for each frequency range revealed that the AUC 0–20 Hz and PH 0–20 Hz comprised 91.5% and 8.1% of the variability in the data. K-means clustering of the unlabeled data generated two main clusters (centroid: [1] x = 0.009, y = 0.019; [2] x = 0.07, y = 0.068) resulting in 97% accuracy of classification per the adjusted Rand index (0.03) (Figure 4G).

Together, these data suggest that the electrophysiological fingerprints of WT and KO mice are significantly different. Given the logical mapping of electrophysiological metrics to physiological parameters of this pathology, with normalization and further development, such metrics can be used to define the regional impact and stage the severity of the condition.

DISCUSSION

Here, we report an electrophysiological tool apt for the anatomical properties of the GI tract and demonstrate the feasibility of the LENS in acquiring stable, luminal electrophysiology in the esophagus and rectum. This tool fundamentally overcomes limitations and challenges of prior methods that involved precarious attachment and stabilization challenges for one or two electrodes.[22] By covering a surface area of ~20 cm with 32 electrodes, the LENS enables spatially mapped electrophysiology as well as localizations of

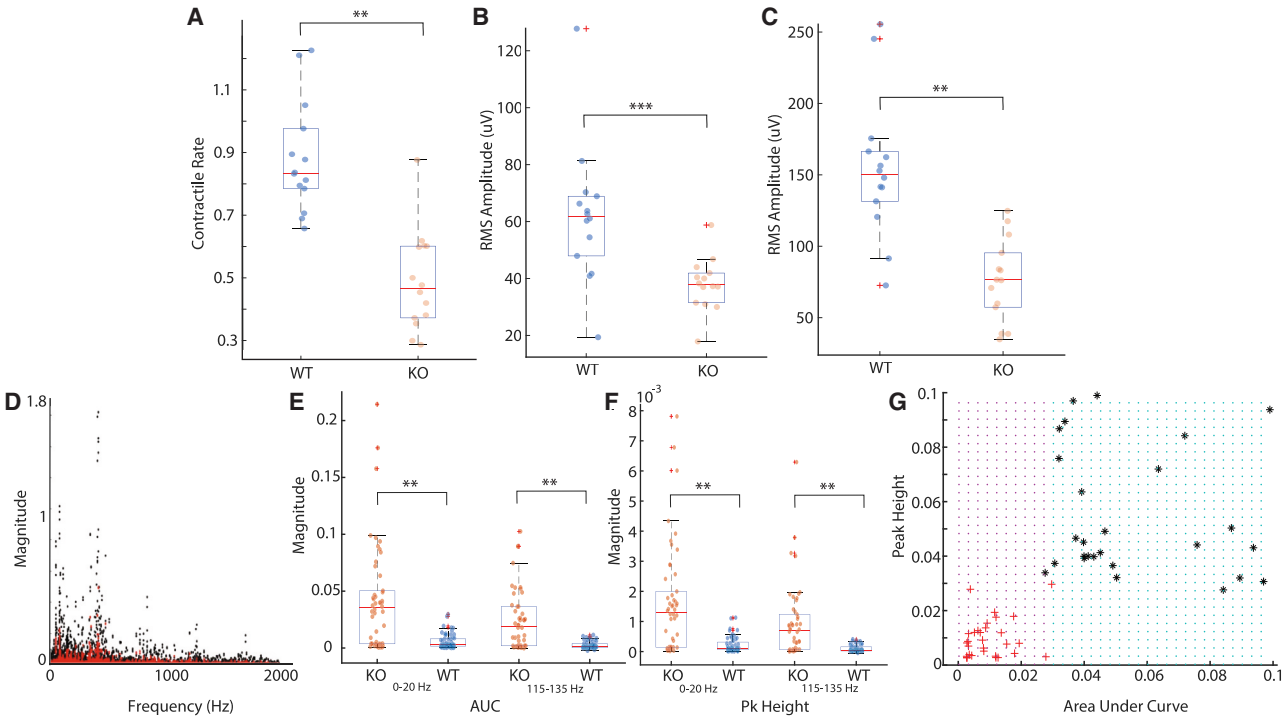

Figure 4. Time domain and frequency spectra profiles for the nNOS model of neuropathy

(A) Contractile rate, the number of bursts per minute, is significantly higher ($p < 0.001$) in WT nNOS mice compared to KO mice.

(B) RMS amplitude of myoelectric activity is significantly higher in WT mice ($p < 0.0001$) compared to KO mice.

(C) With periodic stimulation, the RMS amplitude of WT mice is significantly greater than the KO mice ($p < 0.001$).

(D) Frequency spectra of the myoelectric activity from the WT (red) and KO (black) groups.

(E) Magnitude of the AUC in each frequency band for WT (blue) and KO (orange) mice.

(F) Magnitude of the PH in each frequency band for WT (blue) and KO (orange) mice.

(G) K-means clusters demonstrate two separate regions with 97% accuracy of classification.

lesions with sub-centimeter accuracy. The analytical methods employed here demonstrate new biomarker metrics that can accurately distinguish between ganglionic/aganglionic segments and parametrize neuropathies—providing a basis for clinical diagnostic use of such an electrophysiological tool. In future studies, a greater volume of data as well as testing in other GINMD models will enable the further validation of these biomarkers and development of additional metrics to enable quantitative grading and diagnosis.

For various neuropathic gastrointestinal diseases, current pharmacology is delivered systemically due to a lack of knowledge regarding localized targets. With the LENS, localization of focal areas could enable targeted application of therapeutics such as anesthetics, pro-motility, microbiota, and anti-inflammatory agents. For example, profiling of the small intestine would yield basic insights on disease pathophysiology that can drive the development of new therapies, especially in diseases like irritable bowel syndrome where neural disease is implicated but weakly understood. Additionally, chronic constipation is a large problem for which diagnosis involves a complex, multi-step diagnostic pathway[38] and often leads to nonspecific therapy, given the limitations of current measurement modalities. An electrophysiological profile could help better elucidate the etiology and enable faster determination of the optimal therapy.

While electromyography has been exiguously utilized for decades, the need for simple and physiologically relevant metrics has been emphasized by the clinical community. Such metrics will require a careful understanding of the physiology alongside empirical determination of utility. Previously, mechanical measurements and resting membrane potentials were not able to detect differences between WT and KO nNOS mice,[39] which primarily correspond to muscle activity. Using the LENS, neuromuscular activity, captured by the contractile rate, RMS amplitude, and metrics from the frequency spectra were able to detect significant differences between groups. Although the physiological relevance of these metrics is arbitrary, they serve as a starting point to distinguish healthy and pathological tissues. A multifactorial analysis, composed of such metrics, stands to provide a holistic picture of a given disease phenomenon. In the future, with further data collection, additional analytical methods should be explored, including large-scale regression models. This may help discern subtle differences in the presentation of each disease with common symptoms. While the gel coating significantly improves signal quality, a challenge for a luminal system is motion artifacts. The tool can be further improved to detect motion artifacts or correlate mechanical loss of function (lack of motion artifacts) with neural pathologies.

Table 1. Key resources

Reagent or resource	Source	Identifier
Chemicals, peptides, and recombinant proteins		
Silicone	Sylgard	844
Calcium sulfate	Sigma-Aldrich	255548
Alginate	Sigma-Aldrich	A2033
Acrylamide	Sigma-Aldrich	A8887
N'N-methylenebis (acrylamide)	Sigma-Aldrich	M7279
Free-radical initiator ammonium persulfate	Sigma-Aldrich	A3678
Polymerization accelerator tetramethyl-ethylenediamine	Sigma-Aldrich	T7024
Chitosan	Sigma-Aldrich	448877
1-ethyl-3-(3-dimethylaminopropyl) carbodiimide hydrochloride	Sigma-Aldrich	E1769
n-Hydroxysulfosuccinimide	Sigma-Aldrich	56485
Experimental models: organisms/strains		
Female Yorkshire swine	Cummings Veterinary School at Tufts University	N/A
Mice, male and female	Jackson Labs	B6.129S7-*Ednrb*^{tm1Ywa}/FrykJ B6.129S4-*Nos1*^{tm1Plh}/J
Software and algorithms		
MATLAB 2021b	Mathworks	N/A
ImageJ 2021	NIH	N/A
Other		
Flexible PCBs	PCBway	custom
EndoFlip dilation catheter	Medtronic	ES-330
Gastroscope	Pentax	EG-3470K

The insertion of the probe in the lumen may have mechanically activated mechanosensors in the wall of the tract (sensory neurons, enteric plexus cell bodies, and smooth muscle cells) leading to changes in motility. The LENS incorporates this mechanosensory influence in its profile of healthy and pathologic tissues. With the development of robust GINMD models in large animals, the specific contribution of luminal distention to the changes in motility could be further isolated from the pathology.

Future work should increase the spatial resolution of the device and obtain larger datasets to perform computational analyses. Testing in animal models with chronic gastrointestinal diseases of neural origin would also provide a more robust dataset from which to glean diagnostic metrics. Following further safety and efficacy developments, the LENS would acquire data from individuals, whether healthy or experiencing disease, to determine metrics and values for the specific diagnoses of GINMDs correlated with their subject-specific reports. This tool lays the foundation for both basic scientific insight as well as clinically relevant diagnostics.

EXPERIMENTAL PROCEDURES

Resource availability

Lead contact

Further information and requests for resources should be directed to and will be fulfilled by the lead contact, Shriya Srinivasan (shriyas@mit.edu).

Materials availability

This study did not generate new unique reagents. See Table 1 for details on the materials used.

Data and code availability

- All data are presented within this paper. This paper does not report original code.
- Any additional information required to reanalyze the data reported in this paper is available from the lead contact upon request

Method details

Fabrication of LENS balloon

Flexible PCBs were custom-designed (Altium Designer software) and -manufactured flexPCB (PCBway) on flexible polyimide substrates with copper contacts, as shown in Figure S4. Four electrosensitive strips were placed on a balloon catheter at 0.5-cm intervals longitudinally using biocompatible cyanoacrylate. Each PCB board contained eight equally spaced electrode pads and was connected to an 8G cable containing eight 32G wires. The pointed tip of the PCB boards and the three holes printed near the tip allowed for better adherence and lower delamination risk upon insertion. These flexible PCBs were adhered to an EndoFlip balloon (Medtronic) with medical-grade cyanoacrylate to enable concurrent detection of impedance planimetry and electrophysiology.

Fabrication of LENS sleeve embodiment

A sleeve was fabricated from thermoformed polyurethane, custom sized to a gastroscope (EG- 3470K Gastroscope, Pentax) to which electro- and mechanosensitive flexible PCBs were attached using medical-grade cyanoacrylate. A thin layer of silicone (Sylguard 844) (<0.5 mm) was brushed on top to laminate the PCBs to the surface and prevent detachment during use. The electrode contacts were uncovered.

Formulation of the adhesive hydrogel

Ionic cross-linker calcium sulfate ($CaSO_2$, 255548), alginate (A2033), acrylamide (AAm, A8887), covalent cross-linker N,N′-methylenebis(acrylamide) (MBAA, M7279), free-radical initiator ammonium persulfate (APS, A3678), polymerization accelerator tetramethyl-ethylenediamine (TEMED, T7024), bridging polymer chitosan of medium molecular (448877), the coupling reagents, 1-ethyl-3-(3-dimethylaminopropyl) carbodiimide hydrochloride (EDC, E1769), and n-hydroxysulfosuccinimide (sulfo-NHS, 56485) were purchased from Sigma. Milli-Q (18.3 MΩ) water was used in all experiments.

The fabrication process consisted of 2 steps: (1) the synthesis of dissipative matrix alginate-polyacrylamide (Alg-PAAm) tough hydrogel and (2) adhesive layer coating. The Alg-PAAm tough hydrogel was prepared following a modified protocol based on a previously reported protocol. In brief, sodium alginate powder and AAm were first dissolved in distilled water at 2 wt % and 12 wt %, respectively, and stirred overnight until a clean solution was obtained. After degassing, this prepared pre-gel solution of 10 mL was then mixed with 36 μL of 2 wt % MBAA and 8 μL of TEMED in one syringe (20 mL); 226 μL of 0.27 M APS and 191 μL of 0.75 M $CaSO_4$ slurries were injected into another syringe (20 mL). All bubbles were removed before further cross-linking. After connecting two female Leur adapters (Cole-Parmer), solutions in the two syringes were mixed by pushing the syringe pistons forward and backward 10 times. The mixture was stored inside a closed glass mold at room temperature overnight to allow complete polymerization. After that, hydrogel discs were punched out and adhered to PI film of the flexible PCB on the balloon catheter using biocompatible superglue.

During use, the hydrogel disc surfaces were treated with the bridging polymer and coupling agents for a carbodiimide coupling reaction. The bridging polymer chitosan was dissolved into distilled water at 2.0 wt %, and the pH was adjusted to 5.5–6 by acetic acid. EDC and NHS were used as the coupling reagents. The final concentration of EDC and NHS was 12 mg/mL. The mixture of the bridging polymer and coupling reagents was applied to the surface of the tough hydrogel prior to insertion into the GI tract.

Testing of impedance vs. bending

As the LENS is expected to experience repeated bending during insertion into the target organ and measurement, the durability was tested through a cyclic loading test. Electrode impedance at varying frequencies was measured using the Intan Technologies system prior to and after 1 million cycles of 40% strain imparted at 1 Hz (Instron Bluehill).

Determination of luminal contact

In the balloon catheter embodiment, the level of inflation necessary to maintain stable contact with the lumen was tested using a phased inflation assessment. Briefly, the catheter was inflated with sterile saline in 10-mL increments and allowed to redistribute and stabilize for 2 min prior to recording the impedances (1,000 Hz) on each electrode and overall balloon pressure (Endoflip, Medtronic).

Optimizing curvature

A 20-cm-long, 20-mm diameter balloon catheter was segmented using cylindrical thermoplastic polyurethane strips at equal distances to create 2–5 individual segments. 5-foot-long segments of small intestinal and colonic tissue along with their respective mesenteric membranes were harvested from Yorkshire swine and preserved on ice in their original configuration, with care to ensure that the curvature and dimensions were unaltered. The radii of curvature were measured prior to and after insertion of a standard balloon catheter or segmented catheter. The number of segments, inflation level, and rigidity of the polyurethane cross-sections were optimized to enable the insertion and sliding of the LENS with minimal changes to natural tissue curvature and distention.

Characterization of the properties conferred by the adhesive gel

A coated and uncoated (control) device was placed in an esophagus of a swine, and impedance of the electrodes was measured using the Intan processor (Intan Technologies) at 1,000 Hz. This was repeated for balloon inflation volumes of 5, 10, 20, and 30 mL.

To measure the capability of the adhesive gel to prevent motion, the force required to move the device through the esophagus was measured (Figure S6). A Shimpo FGV-XY digital force gauge was attached to the device, and the esophagus was pulled from the device at a constant rate. Measurements during the initial phase of acceleration were discarded.

In vivo validation

The feasibility of the electrodes to make luminal contact, record key neuromuscular events, and be adaptable to various organs was tested using various GI segments of Yorkshire swine (50–83 kg, $n = 5$). Electrophysiological recordings were carried out on an RHS Stimulation/Recording System (Intan Technologies) at 30-kHz sampling frequency. All large animal *in vivo* procedures were performed in swine under the approval of the Committee on Animal Care at the Massachusetts Institute of Technology (MIT). All small animal procedures were performed under the approval of the IACUC of the Massachusetts General Hospital (MGH, #2009N000239).

Female Yorkshire swine from Cummings Veterinary School at Tufts University (Grafton, MA) were anesthetized with an intramuscular injection of dexmedetomidine (0.03 mg/kg) and midazolam (0.25 mg/kg) and intubated and maintained on 2%–3% isoflurane in oxygen.

Esophagus

The balloon and sleeve embodiments of the LENS were validated against functional lumen imaging (Endoflip, Medtronic) on $n = 3$ swine. Electrical activity on all sensors was recorded during insertion through an overtube placed in the mouth at the UES, proximal esophagus, distal esophagus, and the lower esophageal sphincter (LES). Swallowing activity (natural or reflex-induced) was captured along with tightening of the LES in response to inflation of the balloon catheter after placement. Glucagon (10 units) was intramuscularly injected into the LES using a Carr-Locke needle to induce and capture relaxation. Luminal pressure and stability of contact were assayed throughout the recordings through endoscopic inspection and impedance measurements.

Rectoanal region

Following a 50-mL saline enema, and the inspection of a clean colon, the straight balloon embodiment of the device was inserted up to 25 cm into the rectum. Balloon pressures in relation to inflation were characterized at the anal sphincter. A custom tool to simulate fecal pressure was created and placed in the rectum to induce rectal distension and trigger the rectoanal inhibitory reflex in $n = 2$ swine.

Disease models

We selected two models of intestinal neurogenic disease to demonstrate the utility of spatiotemporal electrophysiology in characterizing physiological characteristics of the organ. (1) nNOS-deficient mice lack nNOS-mediated relaxation in smooth muscle of the GI tract and exhibit delayed gastric emptying and slow transit in the colon. (2) Mice lacking endothelin receptor type B (Ednrb) are a widely used animal model of Hirschsprung disease in which the distalmost segment of colon lacks ENS. The Ednrb mice were crossed with nestin-GFP mice to obtain nestin-GFP; Ednrb-null mice in which enteric glial cells express GFP per Stavely 2021.[40]

Mice of either sex and their WT control littermates (Jackson Laboratory, Maine, USA) were anesthetized using 1%–5% isoflurane.

Following anal dilation, an enema was performed using 2–4 mL of saline. Four to six evenly spaced bipolar electrodes situated on a custom probe (Omnetics) were inserted into the distal colon, and electrical activity was recorded for at least 20 min, Figure S4. A subset was stimulated at 500 or 1,500 μA at 1 and 30 Hz. Upon euthanasia, a laparotomy was performed, and the tissue was inspected for perforation and correct placement of the electrodes (Figure S7). The colon was stained using India ink to mark the most proximal electrode and harvested. Tissue was stained against Tuj1 and nestin-GFP to assess the presence of ganglionic innervation and to identify the TZ in Ednrb mice (Hirschsprung model).

Serosal recordings were also acquired to eliminate potentially interfering factors associated with luminal placement, including the presence of fecal matter, perforation in the tract, and incomplete evacuation of the enema. In Ednrb mice, a laparotomy was performed after the recordings to mark the placement of the electrodes and to distinguish which ones were placed in ganglionic and aganglionic segments to enable identification of the TZ.

Analysis

Data were exported and processed in MATLAB. Data were bandpass and notch filtered (60 Hz) to remove low-frequency motion artifacts, breathing artifacts, and white noise. The data were further rectified and adjusted based on the baseline of the mean rectified signal. The rectified data were smoothed using a 3,000-sample moving window.

Metrics

The RMS amplitude of the data, x, was calculated across time, N, using the following equation:

$$x_{RMS} = \sqrt{\frac{1}{N}\sum_{n=1}^{N}|x_n|^2}, \qquad \text{(Equation 1)}$$

The contractile rate was defined by the number of peaks occurring per unit time. A dormant section of data was manually selected to represent a baseline resting condition. The mean value of these data was designated to be the baseline resting amplitude. Peaks were defined as clusters of spikes at least 1.5 times greater than the baseline resting amplitude and at least 10 ms from the nearest neighbor to prevent double-counting the same spike.

For frequency analysis, data were bandpass filtered between 0.01 and 150 Hz using a second-order Butterworth filter. The DFT of the data was computed using MATLAB's FFT algorithm and enveloped using a 30-sample moving window. Based on clustering analysis, the two most prominent frequency ranges were selected to be 0–20 Hz and 115–135 Hz. The PH and AUC were determined. This was performed for each channel of data recorded from every mouse in each group. A two-tailed heteroscedastic Student's t test was used to evaluate hypotheses related to the physiological parameters of each group.

In addition to significance testing based on *a priori* designations of the (1) nNOS mice into WT or KO categories or (2) electrode placement in a ganglionic or aganglionic region, data were combined and assessed using blinded models. Following the FFT, the PHs in each range and areas under the curve were combined from both WT and KO mice into one large dataset. A principal component analysis was performed to determine the two most influential components. The two largest components were then plotted against each other for all data. K-means clustering was performed and converged consistently within 4 iterations. The adjusted Rand index was calculated to assess the degree of

association between the partition determined by the K-means clustering. In this case, a Rand index of 0 indicates that the clustering accurately differentiated between the two conditions, while a score of 1 would indicate poor clustering or differentiability in the dataset between clusters.[41]

Statistical comparisons were performed using a Student's two-tailed t test after validating normality of the data, unless otherwise indicated.

SUPPLEMENTAL INFORMATION

Supplemental information can be found online at https://doi.org/10.1016/j.device.2024.100400.

ACKNOWLEDGMENTS

We would like to thank the Histology Core facility at the Koch Institute for Integrative Cancer Research at MIT for their assistance with tissue processing. We thank Dr. Kyle Staller for helpful discussions regarding GINMDs. Shriya Srinivasan was supported by funding from the Harvard Society of Fellows. We thank Virginia Fulford for original artwork seen in Figure 1. Binbin Ying is supported by funding from the Banting Postdoctoral Fellowship and NSERC Postdoctoral Fellowship.

AUTHOR CONTRIBUTIONS

S.S.S., B.Y., A.M.G., and G.T. conceived the concept and device. S.L., R.H., S.B., A.A., B.Y., S.S.S., and G.S. created the methodology. S.S.S., A.A., S.L., R.H., S.B., J.K., K.I., J.J., W.A.M.M., A.H., and N.F. performed the experiments. A.M.G., S.S.S., G.T., A.A., S.L., and R.H. contributed to the writing and editing of the manuscript. G.T. and A.M. were responsible for supervision, project management, and funding.

DECLARATION OF INTERESTS

All animal surgeries were reviewed and approved by the Committee on Animal Care at the Massachusetts Institute of Technology.

S.S.S., A.M.G., R.H., and G.T. are co-inventors on provisional patent applications describing the developments presented here. G.T. reports receiving consulting fees from Novo Nordisk. Complete details of all relationships for profit and not for profit for G.T. can be found at the following link: https://dropbox.com/sh/szi7vnr4a2ajb56/AABs5N5i0q9AfT1lqlJAE-T5a?dl=0.

Received: February 28, 2024
Revised: April 1, 2024
Accepted: April 22, 2024
Published: June 18, 2024

REFERENCES

1. Mathias, J.R., and Clench, M.H. (1995). Neuromuscular diseases of the gastrointestinal tract: Specific disorders that often get a nonspecific diagnosis. Postgrad. Med. *97*, 95–108. https://doi.org/10.1080/00325481.1995.11945972.
2. Bernardini, N., Ippolito, C., Segnani, C., Mattii, L., Bassotti, G., Villanacci, V., Blandizzi, C., and Dolfi, A. (2013). Histopathology in gastrointestinal neuromuscular diseases: methodological and ontological issues. Adv. Anat. Pathol. *20*, 17–31. https://doi.org/10.1097/PAP.0b013e31827b65c0.
3. Keller, J., Bassotti, G., Clarke, J., Dinning, P., Fox, M., Grover, M., Hellström, P.M., Ke, M., Layer, P., Malagelada, C., et al. (2018). Advances in the diagnosis and classification of gastric and intestinal motility disorders. Nat. Rev. Gastroenterol. Hepatol. *15*, 291–308. https://doi.org/10.1038/nrgastro.2018.7.
4. Greenberger, N., Blumberg, R., and Burakoff, R. (2015). CURRENT Diagnosis & Treatment Gastroenterology, Hepatology, & Endoscopy, Third Edition 3rd edition (McGraw-Hill Education/Medical).
5. Fox, M.R., Kahrilas, P.J., Roman, S., Gyawali, C.P., Scott, S.M., Rao, S.S., Keller, J., and Camilleri, M.; International Working Group for Disorders of Gastrointestinal Motility and Function (2018). Clinical measurement of gastrointestinal motility and function: who, when and which test? Nat. Rev. Gastroenterol. Hepatol. *15*, 568–579. https://doi.org/10.1038/s41575-018-0030-9.
6. Hansen, M.B. (2002). Small intestinal manometry. Physiol. Res. *51*, 541–556.
7. Triggs, J., and Pandolfino, J. (2019). Recent advances in dysphagia management. F1000Res. *8*, 1527. https://doi.org/10.12688/f1000research.18900.
8. Basilisco, G., and Bharucha, A.E. (2017). High-resolution anorectal manometry: An expensive hobby or worth every penny? Neuro Gastroenterol. Motil. *29*, e13125. https://doi.org/10.1111/nmo.13125.
9. Tack, J., Bisschops, R., and Sarnelli, G. (2004). Pathophysiology and treatment of functional dyspepsia. Gastroenterology *127*, 1239–1255. https://doi.org/10.1053/j.gastro.2004.05.030.
10. Mekaroonkamol, P., Chawla, S., Willingham, F., and Christie, J. (2016). Anorectal Manometry Causing Rectal Perforation: Can We Prevent This Rare Iatrogenic Complication?: 1431. Off. Am. J. Gastroenterol. *111*, S650–S651.
11. Park, J.Y., Choi, P.W., Jung, S.M., and Kim, N.-H. (2016). The Outcomes of Management for Colonoscopic Perforation: A 12-Year Experience at a Single Institute. Ann. Coloproctol. *32*, 175–183. https://doi.org/10.3393/ac.2016.32.5.175.
12. Loeve, A.J., Fockens, P., and Breedveld, P. (2013). Mechanical analysis of insertion problems and pain during colonoscopy: why highly skill-dependent colonoscopy routines are necessary in the first place. and how they may be avoided. Can. J. Gastroenterol. J. Can. Gastroenterol. *27*, 293–302. https://doi.org/10.1155/2013/353760.
13. Perlman, A.L. (2006). Electromyography in oral and pharyngeal motor disorders. GI Motil. Online. https://doi.org/10.1038/gimo32.
14. Angeli, T.R., Du, P., Paskaranandavadivel, N., Sathar, S., Hall, A., Asirvatham, S.J., Farrugia, G., Windsor, J.A., Cheng, L.K., and O'Grady, G. (2017). High-resolution electrical mapping of porcine gastric slow-wave propagation from the mucosal surface. Neuro Gastroenterol. Motil. *29*. https://doi.org/10.1111/nmo.13010.
15. Huizinga, J.D., and Lammers, W.J.E.P. (2009). Gut peristalsis is governed by a multitude of cooperating mechanisms. Am. J. Physiol. Gastrointest. Liver Physiol. *296*, G1–G8. https://doi.org/10.1152/ajpgi.90380.2008.
16. Sha, W., Pasricha, P.J., and Chen, J.D.Z. (2009). Correlations among electrogastrogram, gastric dysmotility, and duodenal dysmotility in patients with functional dyspepsia. J. Clin. Gastroenterol. *43*, 716–722. https://doi.org/10.1097/MCG.0b013e31818b8ed9.
17. Electromyography of the Colon In Situ - Gastroenterology https://www.gastrojournal.org/article/S0016-5085(69)80131-9/fulltext.
18. Cheng, L.K., Nagahawatte, N.D., Avci, R., Du, P., Liu, Z., and Paskaranandavadivel, N. (2021). Strategies to Refine Gastric Stimulation and Pacing Protocols: Experimental and Modeling Approaches. Front. Neurosci. *15*, 645472. https://doi.org/10.3389/fnins.2021.645472.
19. Riezzo, G., Russo, F., and Indrio, F. (2013). Electrogastrography in adults and children: the strength, pitfalls, and clinical significance of the cutaneous recording of the gastric electrical activity. BioMed Res. Int. *2013*, 282757. https://doi.org/10.1155/2013/282757.
20. Gharibans, A.A., Calder, S., Varghese, C., Waite, S., Schamberg, G., Daker, C., Du, P., Alighaleh, S., Carson, D., Woodhead, J., et al. (2022). Gastric dysfunction in patients with chronic nausea and vomiting syndromes defined by a novel non-invasive gastric mapping device. Sci. Transl. Med. *14*, eabq3544. https://doi.org/10.1126/scitranslmed.abq3544.
21. Varghese, C., Schamberg, G., Calder, S., Waite, S., Carson, D., Foong, D., Wang, W.J., Ho, V., Woodhead, J., Daker, C., et al. (2023). Normative Values for Body Surface Gastric Mapping Evaluations of Gastric Motility

Using Gastric Alimetry: Spectral Analysis. Am. J. Gastroenterol. *118*, 1047–1057. https://doi.org/10.14309/ajg.0000000000002077.

22. Marin, A.M., Rivarola, A., and García, H. (1976). Electromyography of the rectum and colon in Hirschsprung's disease. J. Pediatr. Surg. *11*, 547–552. https://doi.org/10.1016/s0022-3468(76)80010-3.
23. Tsuchida, S., and Kimura, Y. (1966). Electromyography of the intestines by the intra-intestinal method. Tohoku J. Exp. Med. *89*, 61–68. https://doi.org/10.1620/tjem.89.61.
24. Frieri, G., Parisi, F., Corazziari, E., and Caprilli, R. (1983). Colonic electromyography in chronic constipation. Gastroenterology *84*, 737–740. https://doi.org/10.1016/0016-5085(83)90139-7.
25. Bayguinov, O., Hennig, G.W., and Sanders, K.M. (2011). Movement based artifacts may contaminate extracellular electrical recordings from GI muscles. Neuro Gastroenterol. Motil. *23*, 1029–e498. https://doi.org/10.1111/j.1365-2982.2011.01784.x.
26. Sanders, K.M., Ward, S.M., and Hennig, G.W. (2017). Extracellular gastrointestinal electrical recordings: movement not electrophysiology. Nat. Rev. Gastroenterol. Hepatol. *14*, 372. https://doi.org/10.1038/nrgastro.2017.39.
27. Helander, H.F., and Fändriks, L. (2014). Surface area of the digestive tract – revisited. Scand. J. Gastroenterol. *49*, 681–689. https://doi.org/10.3109/00365521.2014.898326.
28. Ying, B., Chen, R.Z., Zuo, R., Li, J., and Liu, X. (2021). An Anti-Freezing, Ambient-Stable and Highly Stretchable Ionic Skin with Strong Surface Adhesion for Wearable Sensing and Soft Robotics. Adv. Funct. Mater. *31*, 2104665. https://doi.org/10.1002/adfm.202104665.
29. Kwiatek, M.A., Pandolfino, J.E., Hirano, I., and Kahrilas, P.J. (2010). Esophagogastric junction distensibility assessed with an endoscopic functional luminal imaging probe (EndoFLIP). Gastrointest. Endosc. *72*, 272–278. https://doi.org/10.1016/j.gie.2010.01.069.
30. Lotfollahzadeh, S., Taherian, M., and Anand, S. (2021). Hirschsprung Disease. In StatPearls (StatPearls Publishing).
31. Cheng, L.S., Schwartz, D.M., Hotta, R., Graham, H.K., and Goldstein, A.M. (2016). Bowel dysfunction following pullthrough surgery is associated with an overabundance of nitrergic neurons in Hirschsprung disease. J. Pediatr. Surg. *51*, 1834–1838. https://doi.org/10.1016/j.jpedsurg.2016.08.001.
32. Mashimo, H., and Goyal, R.K. (1999). Lessons from genetically engineered animal models. IV. Nitric oxide synthase gene knockout mice. Am. J. Physiol. *277*, G745–G750. https://doi.org/10.1152/ajpgi.1999.277.4.G745.
33. Mang, C.F., Truempler, S., Erbelding, D., and Kilbinger, H. (2002). Modulation by NO of acetylcholine release in the ileum of wild-type and NOS gene knockout mice. Am. J. Physiol. Gastrointest. Liver Physiol. *283*, G1132–G1138. https://doi.org/10.1152/ajpgi.00192.2002.
34. Anitha, M., Joseph, I., Ding, X., Torre, E.R., Sawchuk, M.A., Mwangi, S., Hochman, S., Sitaraman, S.V., Anania, F., and Srinivasan, S. (2008). Characterization of fetal and postnatal enteric neuronal cell lines with improvement in intestinal neural function. Gastroenterology *134*, 1424–1435. https://doi.org/10.1053/j.gastro.2008.02.018.
35. Terauchi, A., Kobayashi, D., and Mashimo, H. (2005). Distinct roles of nitric oxide synthases and interstitial cells of Cajal in rectoanal relaxation. Am. J. Physiol. Gastrointest. Liver Physiol. *289*, G291–G299. https://doi.org/10.1152/ajpgi.00005.2005.
36. Sivarao, D.V., Mashimo, H., and Goyal, R.K. (2008). Pyloric sphincter dysfunction in nNOS-/- and W/Wv mutant mice: animal models of gastroparesis and duodenogastric reflux. Gastroenterology *135*, 1258–1266. https://doi.org/10.1053/j.gastro.2008.06.039.
37. McCann, C.J., Cooper, J.E., Natarajan, D., Jevans, B., Burnett, L.E., Burns, A.J., and Thapar, N. (2017). Transplantation of enteric nervous system stem cells rescues nitric oxide synthase deficient mouse colon. Nat. Commun. *8*, 15937. https://doi.org/10.1038/ncomms15937.
38. Camilleri, M., Ford, A.C., Mawe, G.M., Dinning, P.G., Rao, S.S., Chey, W.D., Simrén, M., Lembo, A., Young-Fadok, T.M., and Chang, L. (2017). Chronic constipation. Nat. Rev. Dis. Prim. *3*, 17095–17119. https://doi.org/10.1038/nrdp.2017.95.
39. Spencer, N.J. (2013). Characteristics of colonic migrating motor complexes in neuronal NOS (nNOS) knockout mice. Front. Neurosci. *7*, 184. https://doi.org/10.3389/fnins.2013.00184.
40. Stavely, R., Bhave, S., Ho, W.L.N., Ahmed, M., Pan, W., Rahman, A.A., Ulloa, J., Bousquet, N., Omer, M., Guyer, R., et al. (2021). Enteric mesenchymal cells support the growth of postnatal enteric neural stem cells. Stem Cells *39*, 1236–1252. https://doi.org/10.1002/stem.3388.
41. Sinnott, R.O., Duan, H., and Sun, Y. (2016). Chapter 15 - A Case Study in Big Data Analytics: Exploring Twitter Sentiment Analysis and the Weather. In Big Data, R. Buyya, R.N. Calheiros, and A.V. Dastjerdi, eds. (Morgan Kaufmann), pp. 357–388. https://doi.org/10.1016/B978-0-12-805394-2.00015-5.